SolarPACES 2024, 30th International Conference on Concentrating Solar Power, Thermal, and Chemical Energy Systems

Solar Industrial Process Heat and Thermal Desalination

https://doi.org/10.52825/solarpaces.v3i.2327

© Authors. This work is licensed under a Creative Commons Attribution 4.0 International License

Published: 22 Oct. 2025

# Hybrid Concentrated Solar Thermal and Wind Resistive Heating Systems as Key for Competitive Low Emission Industrial Process Heat Generation

Marco Colombi<sup>1,\*</sup> , Paolo Colbertaldo<sup>1</sup>, Matteo Carmelo Romano<sup>1</sup>, and Marco Binotti<sup>1</sup>

<sup>1</sup>Politecnico di Milano, Department of Energy, Italy

\*Correspondence: marco.colombi@polimi.it

Abstract. Concentrated Solar Thermal (CST) has been addressed as a promising technology for industrial heat decarbonization; however, its use is still limited to low-medium temperature processes (50-250°C). The following analysis explores its feasibility at high temperature employing a parabolic trough solar field with a direct two-tank storage configuration using molten salts both as heat transfer fluid and storage medium, to provide a constant 10 MW<sub>TH</sub> power to heat up a process fluid to 500°C. Through an economic optimization, various levels of process decarbonization are examined, also including CST hybridization with resistive electric heating powered by photovoltaic and wind energy generation and computing CO<sub>2</sub> emissions on a life cycle assessment (LCA) basis. The results indicate that CST is a viable alternative to direct electrification up to 30-50% process decarbonization, while hybrid systems show potential to reduce costs up to 40% at high decarbonization levels. Moreover, although achieving 100% process decarbonization remains still unfeasible, decarbonization levels up to 80-95% appear economically viable when considering up-to-date costs and the forecasted carbon tax.

**Keywords:** Process Heat, Solar Thermal, Hybridization, Energy System, Decarbonization

#### 1. Introduction

According to the International Energy Agency (IEA), industrial heat constitutes approximately two thirds of industrial energy demand and nearly one fifth of global energy consumption [1]. Decarbonizing this sector poses a formidable challenge due to the intricate and heterogeneous nature of industrial processes: their diverse temperature requirements, their necessity for onsite heat generation and their unique features often demand tailor-made solutions [2]. In the European Union, the drive towards decarbonization is supported by the Emission Trading System, which currently includes most industrial sectors and plans to eliminate emission allowances by 2034, thus accelerating research and industry efforts toward fully renewable systems [3]. Among the wide spectrum of renewable technologies, Concentrated Solar Thermal (CST) has gathered interest due to its decreasing costs, wide temperature range and higher solar-toheat conversion efficiency, which can halve the land occupation compared to electric heating sustained by photovoltaic technology given the same thermal power output [2] [4]. Despite a significant 45% reduction in costs and increased annual installations between 2010 and 2020 [5], CST is still largely limited to low-medium temperature processes (50-250°C) using pressurized water, steam, or diathermic oil as Heat Transfer Fluids (HTFs) [2]. The slow adoption of CST in industry can be attributed to high upfront costs, low fuel prices in some regions, perceived risks, and an underdeveloped supply chain. Addressing these challenges will require

innovative financial mechanisms, strong policy support, and technological advancements to improve efficiency and reduce CST system costs [2].

The objective of this study is to investigate the pathways for decarbonizing a generic industrial process that operates at medium-high temperature with a constant thermal demand of 10 MW<sub>TH</sub>, required to heat up the process fluid to  $500^{\circ}$ C. Typical processes with similar temperature levels and thermal demands include: glass annealing ( $500\text{-}600^{\circ}$ C, 4-6 MW<sub>TH</sub>), which accounts for 20% of the energy required for glass production; ceramic spray drying ( $450\text{-}600^{\circ}$ C, 2-4 MW<sub>TH</sub>), which constitutes 40% of the energy required for ceramic production; and refinery visbreaking oil cracking ( $450\text{-}550^{\circ}$ C, 10-15 MW<sub>TH</sub>) [6]. The analysis employs a parabolic trough solar field with a direct two-tank storage configuration using molten salts both as heat transfer fluid (HTF) and storage medium, considering also the hybridization with resistive electric heating sustained by photovoltaic (PV) and wind power generation. An economic optimization is conducted to determine the hybrid system's optimal installed capacities under various levels of imposed renewable penetration, benchmarking against a natural gas base case and computing the Levelized Cost of Heat (LCOH), the CO<sub>2</sub> avoidance rate and the Cost of CO<sub>2</sub> Avoided (CCA) considering CO<sub>2</sub> emissions on LCA basis.

## 2. System Modelling

The developed MILP (Mixed Integer Linear Programming) model is based on a year-long simulation with hourly resolution carried out in GAMS using the CPLEX solver, as depicted in *Figure 1*. The model optimizes both system sizing and plant operation, minimizing the LCOH and having as inputs the techno-economic assumptions, the heat load, the imposed renewable penetration (RP) and the hourly energy generation profiles of PV, wind and CST. The latter are assumed to scale linearly at growing installed capacity, which is a continuous variable in the model ( $P_{CST}$ ,  $P_{PV}$  and  $P_{WT}$ ).

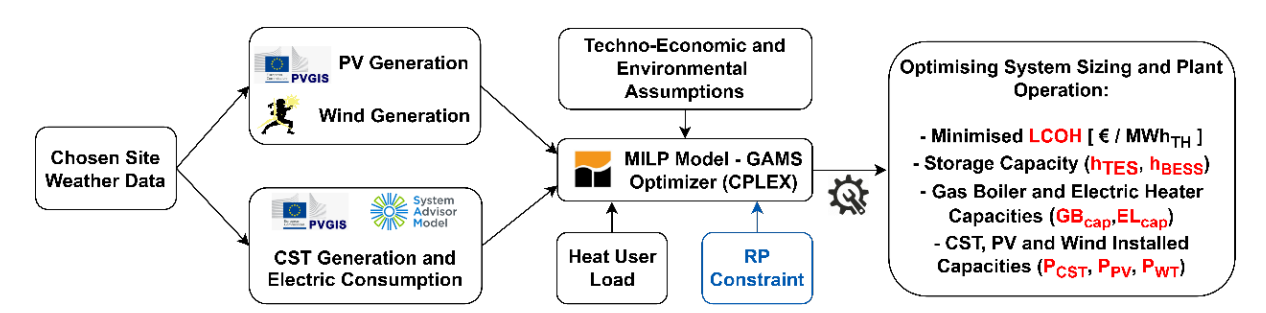


Figure 1. High-level scheme of the optimization logic (optimization variables in red).

The chosen location for the analysis is southern Italy (Taranto, 40.5° N, 17.3° E). The PV generation and weather data for CST are taken from PVGIS [7] using SARAH2 database, while wind generation is taken from [8] using MERRA-2 database. The main parameters of PV and wind generation in the chosen site are reported in *Table 1*.

Table I. Mail	n parameters t	or r v and wind	generation in	the chosen site.	•

Main parameters of DV and wind constation in the change site

Parameter	Value	Parameter	Value	
Annual DNI [kWh/m²/y]	1972	PV / Wind Reference Capacity	2000 kW	
PV Tilt (optimized)	35°	Average Wind Speed	4 m/s	
PV Azimuth (optimized)	-3°	Wind Turbine	Vestas v90 2000	
PV System Loss	15%	Hub Height	80 m	
PV DC Capacity Factor	16.4%	Wind Capacity Factor	33.4%	

The hybrid system has to heat up the process fluid to a temperature  $T_{out}^{proc}$  as illustrated in *Figure 2*. The pinch-point of the heat exchanger between process fluid and molten salts is

assumed on the hot side and equal to  $10^{\circ}\text{C}$ , meaning that the solar field outlet temperature  $T_{out}^{SF}$  will be higher than  $T_{out}^{proc}$  and equal to  $510^{\circ}\text{C}$ . The solar field inlet temperature  $T_{in}^{SF}$  depends on the process fluid inlet temperature  $T_{in}^{proc}$  and is assumed equal to  $400^{\circ}\text{C}$ , though this will be subject to a sensitivity analysis. The CST generation is computed using the SAM tool [9], whose main parameters are reported in Table 2: the design power is set to a medium-high value in order to obtain more representative results; the design DNI is selected considering a 90% value of the DNI cumulative distribution function [10]; and no storage is considered. Two different collector orientations are analyzed, north-south (N-S) and east-west (E-W), to explore the trade-off between a higher annual generation and a lower but more distributed one.

Parameter	Value	Parameter	Value
Collector Type	EuroTrough ET-100	Min Loop Flowrate	1.75 kg/s [11]
Receiver Type	Schott PTR70 (2008)	Max Loop Flowrate	12 kg/s [11]
$T_{in}^{SF}$	400°C	HTF	Hitec Solar Salt
$T_{out}^{SF}$	510°C	n° SCAs per loop	4
$T_{freeze}$	250°C	Collector Azimuth	$0^{\circ} (N-S) - 90^{\circ} (E-W)$
Design DNI	830 W/m <sup>2</sup>	N-S Capacity Factor	15.06%
Design Power	35 MW <sub>TH</sub>	E-W Capacity Factor	13.04%

Table 2. Main parameters for SAM.

### 2.1. MILP Modelling and Renewable Penetration Definition

The system optimization block scheme, depicted in *Figure 2*, presents the following features:

• Each hour, renewable thermal energy is generated either by CST or by PV and wind through an electric heater, and is supplied either directly to meet the process thermal demand or indirectly to charge the thermal energy storage (TES); in case of a shortage, the back-up natural gas boiler covers the residual load heating up molten salts coming from the cold tank  $(Q_{cold})$ . The system is also connected to the electric grid, which however can only provide electricity to the system auxiliaries (solar field pump, freeze protection and tracking systems,  $E_{SF}$ ) and to the hot tank electric resistance to compensate for thermal losses and maintain its temperature constant  $(E_{HT,loss})$ ; the cold tank thermal losses are covered by injecting hot HTF from the hot tank  $(Q_{CT,th})$ . Excess thermal or electric generation can be dumped via defocusing  $(Q_{SF,def})$  or curtailment  $(E_{Ren,curt})$ .

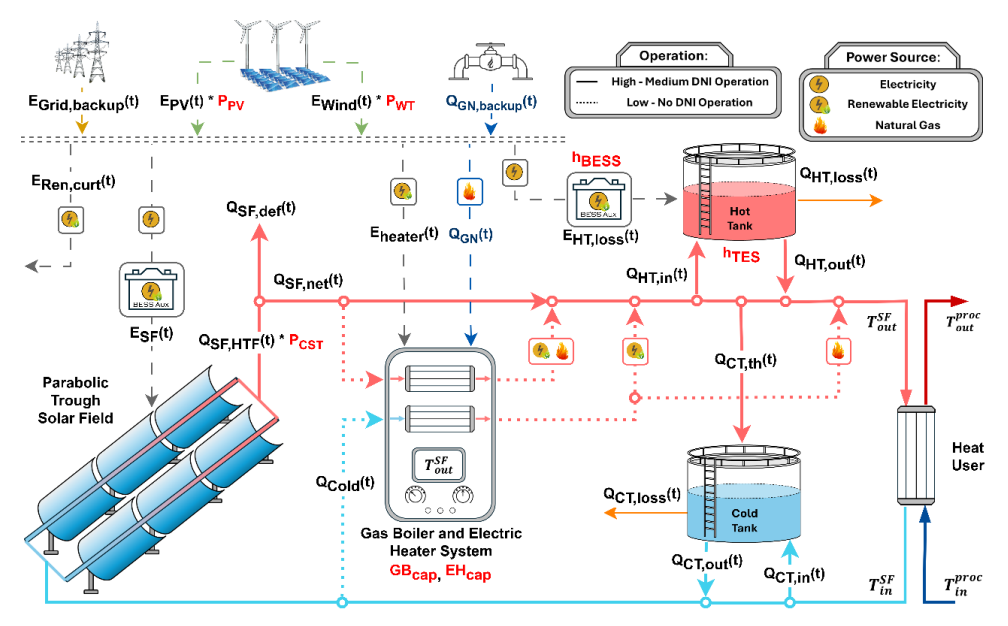


Figure 2. Hybrid system optimization block scheme (optimization variables in red).

- Piping and thermal losses between TES and the heat user are neglected: each light-red or light-blue segment has the same temperature  $T_{out}^{SF}$  or  $T_{in}^{SF}$ , respectively.
- During operation with low DNI, the solar field outlet temperature will be lower than the design value due to the minimum loop flowrate constraint. Assuming that only thermal power at the design temperature  $T_{out}^{SF}$  can be accepted by the heat user, the optimization software can choose whether to discard the CST production in that hour  $(Q_{SF,net})$  or to upgrade it to the design  $T_{out}^{SF}$  using either renewable electricity or natural gas.
- Each TES tank is computed with a 0-D model, considering a uniform temperature across the tank volume. Thermal losses are computed following the SAM approach [9] as shown in Eq. (1), where  $U_{tot}$  is the global heat transfer coefficient and  $A_{tot}$  is the tank surface area. The tank size is optimized keeping a fixed aspect ratio (H/D). Although large-scale molten salt tanks adopt aspect ratios lower than 0.4 due to maximum height constraints [12], being at small-medium scale a value equal to 1 has been considered.

$$Q_{loss}^{tank} = U_{tot} \cdot A_{tot} \cdot (T_{tank} - T_{amb}) \tag{1}$$

- Auxiliary battery energy storage systems (BESS, Li-ion) can be installed to help the system
  achieve an RP equal to 100%, reducing the oversizing of the renewable capacity. The
  BESS can provide electricity just for the system auxiliaries and the hot tank electric resistance.
- The initial state of charge (SoC) of both TES and BESS systems is an optimization variable; a yearly constraint imposes equality between initial and final SoC.

To decarbonize such system, both natural gas and grid electricity use have to be limited. Considering that more than 80% of the system electrical demand is converted into thermal energy by the hot tank resistance and by the solar field freeze protection system, a tailored definition of RP has been developed converting the electric consumption to an equivalent thermal consumption using a reference electric-to-thermal efficiency  $\eta_{el-th}$  equal to 0.99. As shown in Eq. (2), since the annual renewable thermal energy provided to the user  $(Q_{th,load}^{ren})$  is partially produced employing non-renewable electricity from the grid  $(E_{grid}^{non-ren})$  for system auxiliaries, as a penalty the net renewable thermal energy provided to the user  $(Q_{th,load}^{ren,net})$  is considered equal to their difference. As a result, RP is the ratio between  $Q_{th,load}^{ren,net}$  and the annual thermal energy required by the user  $(Q_{th,load})$ , where  $E_{grid}^{non-ren}$  can be found considering the total electricity taken from the grid  $(E_{grid})$  and assuming a renewable penetration in the grid  $(\psi_{grid})$  equal to 50%.

$$RP = \frac{Q_{th,load}^{ren,net}}{Q_{th,load}} = \frac{Q_{th,load}^{ren} - E_{grid}^{non-ren} \cdot \eta_{el-th}}{Q_{th,load}} = \frac{Q_{th,load}^{ren} - (1 - \psi_{grid}) \cdot E_{grid} \cdot \eta_{el-th}}{Q_{th,load}}$$
(2)

## 2.2 Objective Function and Techno-Economic Assumptions

The objective function of the optimization problem is the minimization of the LCOH for each given RP, identifying the optimal renewable installed capacities ( $P_{CST}$ ,  $P_{PV}$  and  $P_{WT}$ ), TES capacity ( $h_{TES}$ ), BESS capacity ( $h_{BESS}$ ) and gas boiler and electric heater capacities ( $GB_{cap}$ ,  $EH_{cap}$ ). The LCOH is computed using Eq. (3), where  $CAPEX_i$ ,  $CCF_i$ ,  $f_{OPEX_i}$  are the installed cost, the carrying charge factor and the annual fixed cost of the i-th component, while  $V_{OPEX}$  accounts for the annual variable operating costs (natural gas, electricity).  $CCF_i$  is computed considering the component lifetime ( $LF_i$ ) and a weighted average cost of capital (WACC) equal to 8% as shown in Eq. (4).

$$LCOH = \frac{\sum_{i} CAPEX_{i} \cdot CCF_{i} + \sum_{i} f_{OPEX,i} + v_{OPEX}}{Q_{th,load}}$$
(3)

$$CCF_i = \frac{WACC \cdot (1 + WACC)^{LF_i}}{(1 + WACC)^{LF_i} - 1} \tag{4}$$

The main techno-economic and environmental assumptions are reported in Table 3. All components are assumed to have a 25-year lifetime except the BESS, for which a 10-year lifetime and 3 substitutions are considered. All specific costs already consider installation, contingencies and indirect costs. The TES cost is taken from SAM (2023) [9] and then adjusted proportionally to the actual  $\Delta T$  between hot and cold tanks following the analysis of Glatzmaier et al. [13]. The cost of the molten salts-heat user heat exchanger is assumed negligible. The natural gas specific CO<sub>2</sub> emissions ( $e_{CO2,GN}$ ) consider also a 0.5% methane leak in the distribution infrastructure, while the grid electricity specific CO<sub>2</sub> emissions ( $e_{CO2,grid}$ ), assumed equal to 200 kg<sub>CO2</sub>/kWh<sub>el</sub>, are representative of a country having the aforementioned renewable penetration (50% average).

**Table 3.** Main technical, economic and environmental assumptions.

Parameter	Value	Ref	Parameter	Value	Ref	
Technical						
[MJ/kg]LHV <sub>NG</sub>	48		Tank H/D Ratio [-]	1		
η <sub>th,gas boiler</sub> [-]	0.90	[14]	BESS η <sub>charge-discharge</sub> [-]	0.97		
ηel-th, heater / resistance [-]	0.99		BESS η <sub>self-discharge</sub> [h <sup>-1</sup> ]	10-4		
Tank U <sub>tot</sub> [W/m <sup>2</sup> K]	0.4		BESS t <sub>charge-discharge</sub> [h]	3		
Economic						
CCF <sub>25 Years</sub> [1/y]	0.094		TES Cost Δ <i>T</i> =265°C [€/kWh]	20.7	[9]	
CCF <sub>30 Years (BESS)</sub> [1/y]	0.089		f <sub>OPEX,MS</sub> tes [% <sub>CAPEX</sub> ]	2 %		
PV Cost [€/kW <sub>DC</sub> ]	700	[15]	BESS Cost [€/kWh]	250	[15]	
f <sub>OPEX,PV</sub> [% <sub>CAPEX</sub> ]	2 %	[15]	f <sub>OPEX,BESS</sub> [% <sub>CAPEX</sub> ]	2.5 %	[16]	
Wind Cost [€/kW]	1400	[15]	NG Boiler Cost [€/KW <sub>TH</sub> ]	82	[14]	
f <sub>OPEX,Wind</sub> [% <sub>CAPEX</sub> ]	3 %	[15]	f <sub>OPEX,NG Boiler</sub> [% <sub>CAPEX</sub> ]	2.5 %		
CST Cost [€/m²]	250	[9]	EL Heater Cost [€/KW <sub>TH</sub> ]	50	[17]	
f <sub>OPEX,CST</sub> [% <sub>CAPEX</sub> ]	2.5 %		f <sub>OPEX,EL Heater</sub> [% <sub>CAPEX</sub> ]	1 %		
TES Cost Δ <i>T</i> =110°C [€/kWh]	50.0	[9]	NG Cost [€/MWh <sub>LHV</sub> ]	40	[18]	
TES Cost Δ <i>T</i> =210°C [€/kWh]	26.1	[9]	Electricity Cost [€/MWhel]	160	[19]	
Environmental						
[-]ψ <sub>grid</sub>	0.5		$LCA_{Wind} [kg_{CO2,eq}/kW]$	557		
[kg <sub>CO2,eq</sub> /MWh <sub>NG</sub> ]e <sub>CO2,GN</sub>	213		LCA <sub>Solar Field</sub> [kg <sub>CO2,eq</sub> /m <sup>2</sup> ]	145		
[kg <sub>CO2,eq</sub> /MWh <sub>EL</sub> ]e <sub>CO2,grid</sub>	200		LCA <sub>TES</sub> [kg <sub>CO2,eq</sub> /m <sup>3</sup> ]	1260		
LCA <sub>PV</sub> [kg <sub>CO2,eq</sub> /kW]	600		LCA <sub>BESS</sub> [kg <sub>CO2,eq</sub> /kWh]	70		

The natural gas base case is represented by RP equal to 0, where molten salts are heated using only the 10 MW<sub>TH</sub> NG boiler. The CO<sub>2</sub> avoidance rate is computed from the ratio between the avoided and the base case annual CO<sub>2</sub> emissions. The Cost of CO<sub>2</sub> Avoided (CCA), defined in Eq. (5), is computed as the ratio between the annual cost and the CO<sub>2</sub> emission differentials between hybrid and base case.  $\Delta C_{inv,i}^{Hybrid-Base}$  is the cost differential of the *i*-th technology,  $\Delta C_{EL}^{Hybrid-Base}$  and  $\Delta C_{GN}^{Hybrid-Base}$  are the cost differentials of electricity and natural gas consumptions, while  $e_{CO_2}^{Base}$  and  $e_{CO_2}^{Hybrid}$  are the specific CO<sub>2</sub> emissions of the base and hybrid cases.

$$CCA = \frac{\sum_{i} CCF_{i} \cdot \Delta C_{inv,i}^{Hybrid-Base} + \Delta C_{EL}^{Hybrid-Base} + \Delta C_{GN}^{Hybrid-Base}}{\left(e_{CO_{2}}^{Base} - e_{CO_{2}}^{Hybrid}\right) \cdot Q_{th,load}}$$
(5)

Considering  $CO_2$  emissions on LCA basis, the  $CO_2$  avoidance rate considers not only the direct emissions associated with NG combustion, but also the indirect ones associated to methane leakage, to grid electricity generation and delivery and to the embedded carbon in renewable energy technologies, while CCA just considers direct and grid electricity emissions.

#### 3. Results

Four different cases are analyzed and the LCOH cost breakdown, the CO₂ avoidance rate and the CCA are shown in *Figure 3*. Due to the electricity demand required for the solar field auxiliaries, the CST case is limited to RPs lower than 90% and exhibits a very steep gradient already at RP=60%, highlighting the drawbacks of relying just on one technology. Given the current set of assumptions, CST is more advantageous than PV due to its lower specific cost (443 versus 700 €/kW<sub>peak</sub>). However, in the CST+PV case, CST is outperformed by PV at medium-high RP due to its lower seasonal capacity factor and availability during winter, which are key factors in determining the storage capacity and renewable overcapacity to be installed. On the contrary, the decorrelated CST and wind hourly generation leads to significant improvement in terms of LCOH, since the overnight wind electricity generation favors CST adoption, which is cheaper than PV, covering CST solar field auxiliaries and delaying BESS adoption to higher RPs. The CST+PV+WT case shows the lowest LCOH for RPs between 80% and 100%, where the CST capacity greatly reduces due to the aforementioned reason.

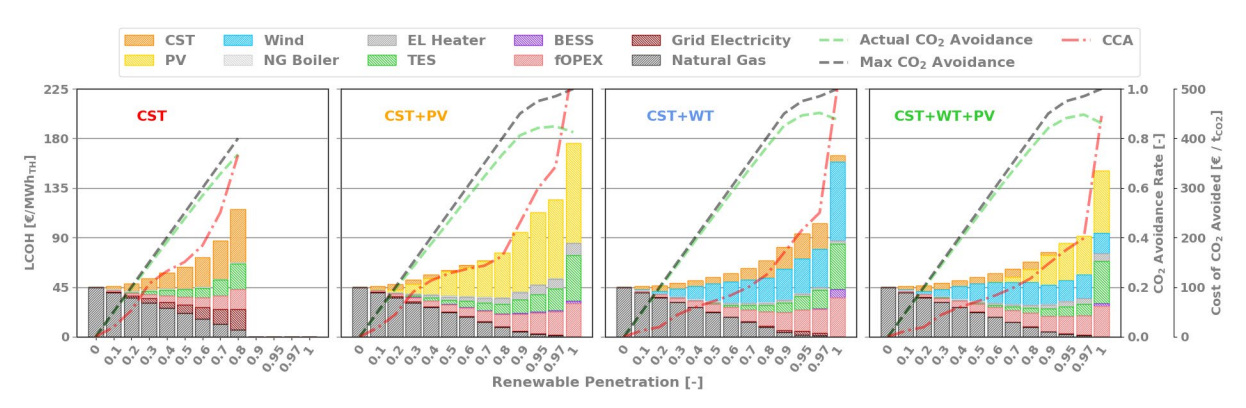


**Figure 3.** LCOH cost breakdown, CO<sub>2</sub> avoidance rate and Cost of CO<sub>2</sub> Avoided for each RP considering CST only and CST hybridization with PV and Wind. The black dashed line, directly proportional to RP, is not linear between 90% and 100% RP due to the x-axis step variation.

The black and green dashed lines in Figure 3 represent the direct and actual CO₂ avoidance rate, respectively, where the latter accounts also for LCA emissions. Despite achieving a 100% renewable system in energy terms, the embedded CO₂ associated with renewable energy technologies leads to decarbonization rates of up to 90%. The short-term ETS carbon price forecasts range between 100 and 150 €/tco₂ [20], which, if compared with the red dashed lines showing the CCA, make renewable heat generation competitive up to an RP of 80-90% for CST+WT and CST+PV+WT cases in the current techno-economic framework. The installed capacities for each case are shown in Figure 4, where the colored symbol on top of each stacked column represents the optimized collector orientation.

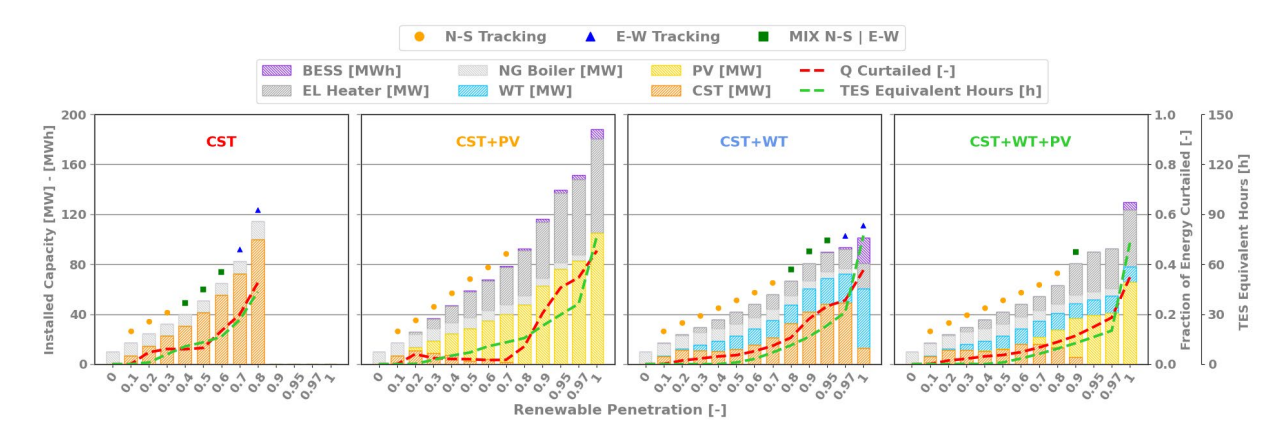


**Figure 4.** Installed capacities, solar field orientation, curtailed energy fraction (thermal + electric) and TES equivalent hours for each RP considering CST only and CST hybridization with PV and Wind.

As it can be seen, at low RPs the N-S orientation is preferred due to the higher annual energy yield while at high RPs the E-W orientation is chosen due to the more uniform generation along the year, which greatly reduces the storage capacity needed. In the mid-range RPs a mix between N-S and E-W orientations is preferred to exploit both their advantages, with the fraction of E-W compared to N-S growing when moving towards high RPs. In the CST case, at high RP, the optimal NG boiler capacity exceeds the heat user nominal power due to the need to upgrade the molten salts from the solar field during low DNI hours. Similarly, in hybrid cases the EL heater capacity is oversized in order to exploit and then store the renewable electricity overgeneration. The red dashed lines in Figure 4 represent the curtailed fraction of renewable energy, which is the ratio between the sum of the solar field defocused energy and the curtailed PV and wind energy over the total renewable energy generated. The green dashed lines represent the TES equivalent hours, computed as the ratio between the TES thermal capacity and the heat user requested power. As can be seen, the higher the RP the higher the renewable overcapacity installed and consequently the fraction of energy curtailed and the TES equivalent hours. In particular, the increase in TES capacity between RP 97% and 100% is remarkably steep, showing how difficult it is to reach a fully renewable system.

It is important to emphasize that these results were obtained under the assumption of no land availability constraints and negligible land costs, as PV and wind energy generation may be delocalized through Power Purchase Agreements (PPAs), unlike CST. In the on-site CST+PV scenario, land constraints will inevitably limit the feasibility of achieving very high RPs, with CST likely being favored over PV due to its higher power density and thus lower specific land occupation (6.5 vs 12.1 m²/kW<sub>TH</sub> [21] [22] [23]). Regarding the impact of land costs on LCOH, in the analysed 510-400°C on-site CST+PV case, assuming a land cost equal to 10 €/m2, increasing RP from 0.1 to 1 results in a LCOH increase of only 1 to 7%.

Important variables to be optimized are the solar field inlet and outlet temperatures  $T_{in}^{SF}$  and  $T_{out}^{SF}$ , whose influence on the levelized cost of renewable heat (LCOH<sub>REN</sub>) and on the installed capacities is shown in Figure 5 for the CST+WT+PV case.

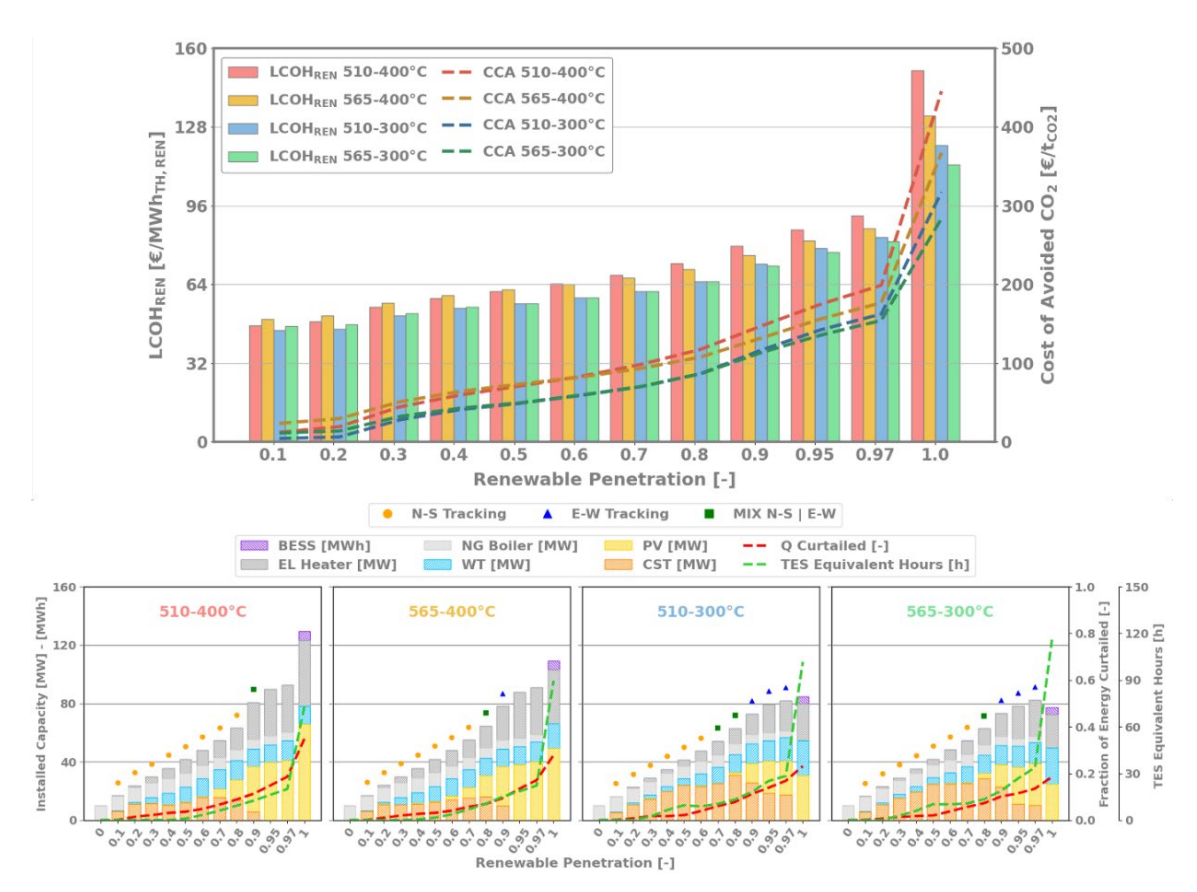


**Figure 5.** Solar field inlet and outlet temperature effect on: (upper) LCOH<sub>REN</sub> and CCA; (lower) Installed capacities, solar field orientation and TES equivalent hours for the CST+WT+PV hybrid system.

The solar field  $\Delta T$  directly influences the CST thermal efficiency and the storable energy per unit volume of TES, which is proportional to the TES specific cost as mentioned in Section 2.2. Increasing the solar field  $\Delta T$ , in particular reducing the  $T_{in}^{SF}$  to 300°C, makes the share of CST capacity increase due to two main reasons: i) the solar field operates at a lower average temperature, increasing CST thermal efficiency, and ii) following the trade-off between generation and storage costs, which favored PV over CST at high RPs in the reference case, a reduction in TES costs shifts the preference toward CST, whose lower generation costs offset its higher storage requirements. As a result, increasing the solar field  $\Delta T$  from 110°C to 210-265°C, the LCOH<sub>REN</sub>, which neglects natural gas and electricity costs and is equal to LCOH at 100% RP, presents an average 10% reduction and the hybrid system becomes competitive up to an RP of 90-95%.

#### 4. Conclusion

This analysis investigated the techno-economic and environmental performances of different decarbonization levels for a generic medium-high temperature industrial process employing hybrid CST-resistive heating system sustained by PV and wind, obtaining the following results:

- Despite the moderate annual DNI of the chosen site (1972 kWh/m²/y), CST proves to be a
  valid alternative to direct electrification for low-medium RPs, despite being outperformed
  by PV at medium-high RP due to its lower seasonal capacity factor and availability during
  winter, which are key factors in determining the storage capacity and renewable overcapacity to be installed;
- One of the CST drawbacks when employing molten salts is the high auxiliary electricity
  consumption, given mostly by the freeze protection system, which limits the system capability to reach high renewable penetrations. This could be tackled by recirculating HTF from
  the cold tank in the field during night, avoiding freeze protection at the expense of lowering

the cold tank temperature, accepting harsher start-up heating transients during the morning;

- CST hybridization, especially with wind energy due to the complementary availability curves, is crucial to lower investment costs and minimize the LCOH, as shown by the 40% LCOH reduction at RP 80% for the CST+PV+WT case with respect to the CST case;
- The solar field temperature difference has a moderate impact on the CST thermal efficiency and on the TES specific cost. Increasing the solar field ΔT from 110°C to 210-265°C yields an average reduction of 10% of the renewable LCOH;
- Although it is possible to achieve a 100% renewable penetration, the embedded CO<sub>2</sub> in the renewable energy technologies leads to decarbonization rates of up to 90% compared to the natural gas-fired benchmark;
- Under current short-term market conditions and in the absence of CO₂ pricing or policy frameworks like the EU ETS, process heat decarbonization using CST, PV, and wind is generally not cost-competitive beyond modest levels (up to 10–20% RP) compared to conventional gas-fired boilers. Conversely, considering the short-term forecasted ETS carbon price range of 100-150 €/t<sub>CO2</sub>, decarbonization levels up to 80-90% are economically viable in the CST+WT and CST+PV+WT cases with 510-400°C fluid temperatures, increasing up to 95% when considering a solar field ΔT equal to 210 or 265°C.

## Data availability statement

Data will be made available on request.

#### **Author contributions**

**Marco Colombi**: Methodology, Investigation, Formal analysis, Software, Visualization, Writing – original draft. **Paolo Colbertaldo**, **Matteo C. Romano** and **Marco Binotti**: Conceptualization, Methodology, Supervision, Validation, Writing – review & editing.

# **Competing interests**

The authors declare that they have no competing interests.

#### References

- [1] IEA (2018), Clean and efficient heat for industry, IEA, Paris <a href="https://www.iea.org/commentaries/clean-and-efficient-heat-for-industry">https://www.iea.org/commentaries/clean-and-efficient-heat-for-industry</a>.
- [2] C. Schoeneberger, C. McMillan, P. Kurup, S. Akar, R. Margolis, E. Masanet, "Solar for industrial process heat: A review of technologies, analysis approaches, and potential applications in the United States", Energy, Volume 206, 2020, <a href="https://doi.org/10.1016/j.energy.2020.118083">https://doi.org/10.1016/j.energy.2020.118083</a>.
- [3] European Commission, EU ETS, <a href="https://climate.ec.europa.eu/eu-action/eu-emissions-trading-system-eu-ets">https://climate.ec.europa.eu/eu-action/eu-emissions-trading-system-eu-ets</a> it (Accessed July 26, 2024).
- [4] O. Marzouk, "Land-Use competitiveness of photovoltaic and concentrated solar power technologies near the Tropic of Cancer", Solar Energy, Volume 243, 2022, Pages 103-119, <a href="https://doi.org/10.1016/j.solener.2022.07.051">https://doi.org/10.1016/j.solener.2022.07.051</a>.
- [5] IRENA (2021), Renewable Power Generation Costs in 2020, International Renewable Energy Agency, Abu Dhabi.
- [6] M. D'Auria, M. Lanchi, R. Liberatore, "Selezione delle configurazioni di sistemi solari a concentrazione idonei alla fornitura di calore di processo per diversi settori applicativi industriali ed elaborazione di schemi concettuali di integrazione", 2019, ENEA.

- [7] T. Huld, R. Müller, A. Gambardella, "A new solar radiation database for estimating PV performance in Europe and Africa", Solar Energy, Volume 86, Issue 6, 2012, Pages 1803-1815, <a href="https://doi.org/10.1016/j.solener.2012.03.006">https://doi.org/10.1016/j.solener.2012.03.006</a>.
- [8] I. Staffell, S. Pfenninger, "Using Bias-Corrected Reanalysis to Simulate Current and Future Wind Power Output". Energy 114, pp. 1224-1239, 2016, <a href="https://doi.org/10.1016/j.energy.2016.08.068">https://doi.org/10.1016/j.energy.2016.08.068</a>.
- [9] System Advisor Model Version 2023.12.17 (SAM 2023.12.17). National Renewable Energy Laboratory. Golden, CO. Accessed July 26, 2024. <a href="https://sam.nrel.gov/download.html">https://sam.nrel.gov/download.html</a>
- [10] M. Wagner, «SAM Webinar: Modeling Parabolic Trough Systems,» NREL, 2014.
- [11] M. Wagner, «SAM Webinars: Modeling Molten Salt Power Tower Systems,» NREL, 2017.
- [12] E. González-Roubaud, D. Pérez-Osorio, C. Prieto, "Review of commercial thermal energy storage in concentrated solar power plants: Steam vs. molten salts", Renewable and Sustainable Energy Reviews, Volume 80, 2017, Pages 133-148, <a href="https://doi.org/10.1016/j.rser.2017.05.084">https://doi.org/10.1016/j.rser.2017.05.084</a>.
- [13] G. Glatzmaier, "Developing a Cost Model and Methodology to Estimate Capital Costs for Thermal Energy Storage", NREL, 2011.
- [14] J. Pérez, A. Jaramillo, M. García, J. Cardemil, R. Escobar, "Techno-economic analysis of hybrid solar thermal systems with flat plate and parabolic trough collectors in industrial applications", Alexandria Engineering Journal, Volume 86, 2024, https://doi.org/10.1016/j.aej.2023.11.056.
- [15] IRENA (2024), Renewable power generation costs in 2023, International Renewable Energy Agency, Abu Dhabi.
- [16] NREL (National Renewable Energy Laboratory). 2022. "2022 Annual Technology Baseline." Golden, CO. https://atb.nrel.gov/electricity/2022/utility-scale battery storage
- [17] D. Stack, D. Curtis, C. Forsberg, "Performance of firebrick resistance-heated energy storage for industrial heat applications and round-trip electricity storage", Applied Energy, Volume 242, 2019, Pages 782-796, <a href="https://doi.org/10.1016/j.apenergy.2019.03.100">https://doi.org/10.1016/j.apenergy.2019.03.100</a>.
- [18] GME, «Gestore Mercati Energetici,» [Online]. Available: <a href="https://www.mercatoelettrico.org/it/">https://www.mercatoelettrico.org/it/</a>.
- [19] Eurostat, Electricity prices for non-household consumers, accessed: 12/7/24, <a href="https://ec.europa.eu/eurostat">https://ec.europa.eu/eurostat</a>.
- [20] BloombergNEF, EU ETS Market Outlook 1H 2024: Prices Valley Before Rally, (accessed: 08/08/24) <a href="https://about.bnef.com/blog/eu-ets-market-outlook-1h-2024-prices-valley-before-rally/">https://about.bnef.com/blog/eu-ets-market-outlook-1h-2024-prices-valley-before-rally/</a>.
- [21] solarthermalworld.org, "Solar Thermal Shows Highest Energy Yield Per Square Metre", accessed: 19/05/25, <a href="https://solarthermalworld.org/news/solar-thermal-shows-highest-energy-yield-square-metre/">https://solarthermalworld.org/news/solar-thermal-shows-highest-energy-yield-square-metre/</a>
- [22] M. Bolinger and G. Bolinger, "Land Requirements for Utility-Scale PV: An Empirical Update on Power and Energy Density," *IEEE J Photovolt*, vol. 12, no. 2, pp. 589–594, Mar. 2022, doi: 10.1109/JPHOTOV.2021.3136805.
- [23] S. Ong, C. Campbell, P. Denholm, R. Margolis, and G. Heath, "Land-Use Requirements for Solar Power Plants in the United States," 2013. [Online]. Available: <a href="https://www.nrel.gov/publications">www.nrel.gov/publications</a>.